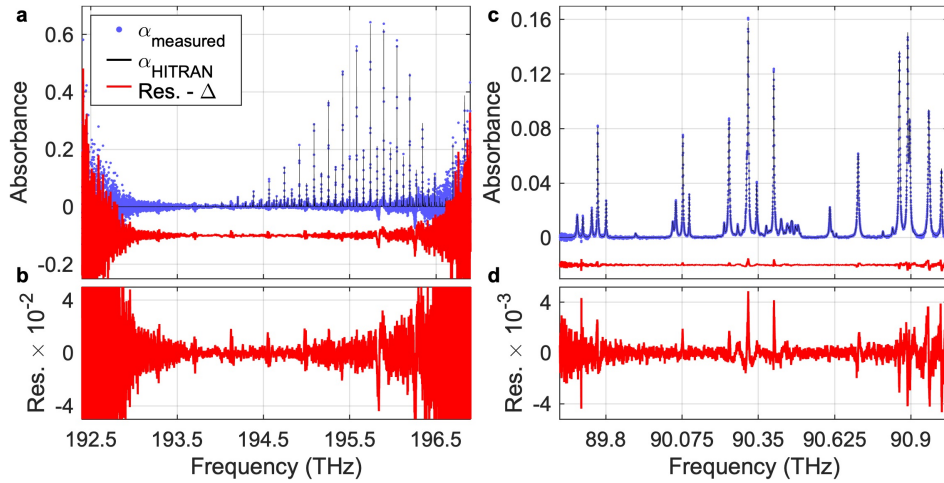# Supplementary information

1 Detailed analysis of the residuals of the SWIR DCS and the ambient pressure CCS measurement

In this section, we further examine the absorbance and residuals (compared to the HITRAN database) for the gas sample measurements presented in the main text. Supplementary Fig. 1a,c show the SWIR-DCS and midIR-CCS measurements from the main text, respectively, and Supplementary Fig. 1b and 1d show the corresponding zoomed-in residuals.

Supplementary Fig. 1 Left column: SWIR DCS measurement on a low-pressure acetylene cell (see Supplementary Fig. 6 in the Results section for more details). Right column: CCS measurement on ambient air (see Supplementary Fig. 10 in the Results section for more details).
(a) and **(c)** Measured absorbance spectrum (blue) compared with HITRAN calculations (black), the residuals are shown by the red curve, which is displaced from 0 for visibility. **(b)** and **(d)** Zoomed-in residuals.

At the edges of the measured spectrum the magnitude of the residuals increases because of the reduced power in the spectral wings which leads to an increase of the noise floor. The magnitude of the residuals relative to the peak absorbance is below 3.5% for the SWIR DCS measurement and below 3.1% for the CCS measurement in

the range not dominated by noise (193.2-195.8 THz and 89.7-90.9 THz, respectively). The respective standard deviation of the residuals is 4.7×10^{-3} and 5.6×10^{-4}.

In the SWIR DCS measurement, systematic artifacts can be found at frequencies spaced by 0.42 THz. As briefly discussed in the results section of the main text, these features are most likely caused by a polarization rotation effect introduced by an intra-cavity height change of the two combs. The reason we attribute these artifacts to depolarization is based on the observation that their frequency spacing corresponds to the delay expected from the difference of the ordinary and extraordinary group index n_{g} of the PPLN crystal at the signal wavelength:

$$\Delta f = \frac{c}{2L_{\mathrm{PPLN}}(n_{\mathrm{g,o}} - n_{\mathrm{g,e}})}. \tag{1}$$

The factor 2 accounts for the linear cavity where the resonant beam is transmitted through the nonlinear crystal twice. The polarization of the resonant beam can be partly rotated when the beam height varies strongly between two reflective intra-cavity optics hit at an angle in the horizontal plane. In the birefringent nonlinear crystal, the projections of the polarization state on the respective crystal axis experience different group indices n_{g}. This creates a small p-polarized pulse delayed relative to the main s-polarized pulse. Although the delayed pulse is not amplified, it builds up resonantly in the OPO cavity. Based on the Sellmeier relation of the crystal [1], the observed frequency spacing is consistent with a 4.3-mm-long PPLN crystal, which is close to the nominal length specified by the manufacturer. Such polarization related spectral artifacts are not present on the CCS measurements because of the temporal filtering effect of mixing with the pump, which cleans up the idler pulses compared to the signal. Distortions in the absorbance associated with such polarization effects could be mitigated by carrying out sample-free reference measurements.

2 Low-pressure CCS measurement

To demonstrate the suitability of the source for high-resolution measurements, we conducted two more measurements on a 65-mbar acetylene cell where the absorption features have a width ~ 1 GHz. Firstly, the idler center wavelength is set to 3792 nm, at the wings of a strong acetylene absorption feature. In this spectral band also water has some weak absorption lines. The results of this measurement are shown in Supplementary Fig. 2a-d. This measurement has a SNR of 36.5 dB, $\sigma_H = 2.2 \times 10^{-4}$ for a 10-ms-long measurement, corresponding to 46.6 dB Hz$^{1/2}$, and a FOM of 1.3×10^8 Hz$^{1/2}$. The SNR is limited by the available idler power, which is reduced because the sample cell is not ideally suited for mid-IR measurements: it has fused silica windows which are absorbing in the wavelength range >2400 nm. The measurement shows good agreement with the HITRAN database. The standard deviation of the residuals is 7.1×10^{-4} in a 1.2 THz wide segment centered about the peak.

In a second measurement, the idler center wavelength is set to 2959 nm, where acetylene has a weak absorption feature. The results of this measurement are shown in Supplementary Fig. 2e-h. The measurement has a SNR of 40.1 dB, $\sigma_H = 9.7 \times 10^{-5}$, corresponding to 50.2 dB Hz$^{1/2}$, and a FOM of 3.4×10^8 Hz$^{1/2}$. The measurement

shows good agreement with the HITRAN database, as well. The standard deviation of the residuals is 1.6×10^{-3} in a 1.2 THz wide segment centered about the peak.
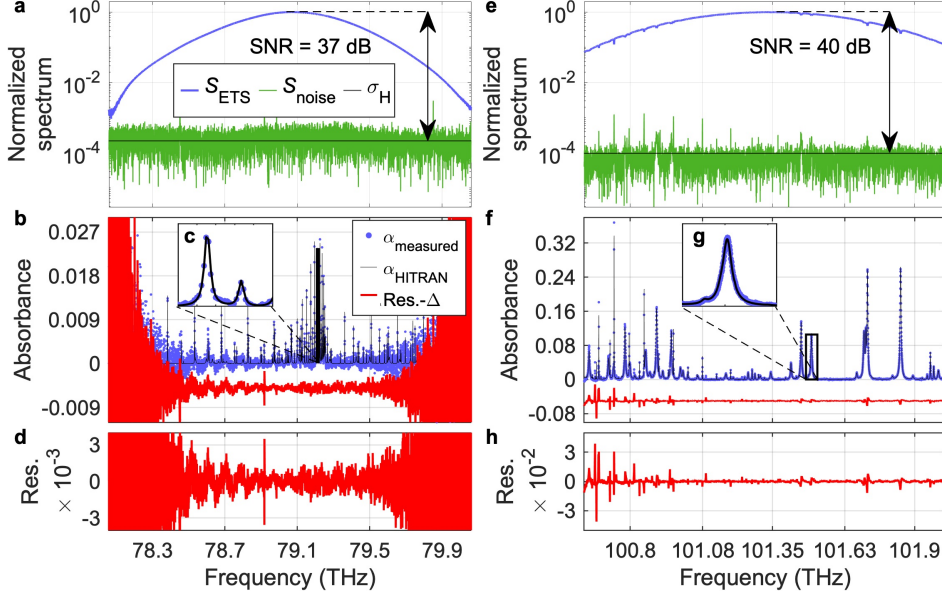
Supplementary Fig. 2 CCS measurements on a low-pressure acetylene cell. Left column: Measurement around 3792 nm. Right column: Measurement around 2959 nm.
(a) Measured spectrum (blue) and its noise floor (green). The blue curve is obtained from $y_{\text{ETS}}(t)$ over the time range from -20 ps to 2000 ps. The green curve is obtained from $y_{\text{noise}}(t)$ over the full time range except for the small region around $T = 0$ where the stitching occurs at 6 ps.
(b) Measured absorption spectrum (blue) compared with HITRAN calculations (black). The residuals are shown by the red curve, which is displaced from 0 for visibility.
(c) Zoom-in on the absorption features to highlight the good agreement of the measurement with HITRAN. α_{HITRAN} is calculated with a sampling rate corresponding to the resolution of the measured data.
(d) Zoomed-in residuals.
Corresponding information for **(e-h)**. The blue curve is obtained from $y_{\text{ETS}}(t)$ over the time range from -50 ps to 2800 ps. The stitching occurs at 20 ps.

To obtain the best overlap with the HITRAN data base, we account for the cell temperature, deviations from the manufacturer-specified pressure, as well as an off-center beam path through the sample cell that falls within the provided tolerances. In the CCS measurements, we also account for atmospheric absorption of methane and water. The relevant parameters are summarized in Supplementary Table 1 for all spectroscopic measurements presented. The nominal values for the cell are: $L_{\text{nom}} = 14 \pm 3$ mm and $p_{\text{nom}} = 66 \pm 13$ mbar

We attribute the elevated temperature and pressure of the acetylene cell in the CCS measurements to the strong absorption of UVFS at the idler wavelength. The fractions for water and methane are found by keeping the interaction length of the idler with the atmosphere fixed to a value found by measuring the path length with

Supplementary Table 1 Summary of the parameters for the HITRAN-based absorbance calculation for all spectroscopic measurements performed.

Parameter	Symbol	Unit	DCS 1540 nm	CCS 2959 nm	CCS 3320 nm	CCS 3792 nm
Cell pressure	p_{cell}	mbar	67.9	78.5	-	79
Cell temperature	T_{cell}	°C	23	42.9	-	43.9
Cell distance	L_{cell}	mm	13.4	13.2	-	13.6
Air pressure	p_{air}	mbar	-	≈ 950	≈ 950	≈ 1000
Air temperature	T_{air}	°C	-	23	25	23
Air distance	L_{air}	m	-	2.68	2.71	2.68
Fraction H$_2$O	$F_{\text{H}_2\text{O}}$	%	-	1.01	1.05	1.52
Fraction CH$_4$	F_{CH_4}	ppm	-	-	2.5	-

a ruler. All measurements have been conducted on different days such that variations in the air humidity can be expected. For the measurements using the acetylene cell, the optical alignment and cell placement have changed in between the measurements, such that the exact path through the cell was not preserved.

3 Coherence of the SWIR DCS measurement

In Supplementary Fig. 3, we show how the SNR of our measurement scales by $\sigma_H \propto T^{-1/2}$ [2], where T is the measurement time.
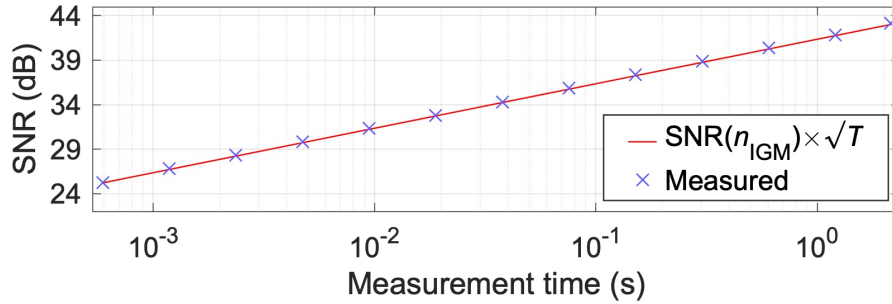
Supplementary Fig. 3 SNR as a function of the measurement time T (blue crosses), compared to the SNR of a single IGM scaled with $\sqrt{T}$ (red).

# 4 Phase tracking with low Δf_{rep}

The OPO-signal pulse stacking setup of Supplementary Fig. 5 in the main manuscript mimics the role of a larger Δf_{rep} by sampling the phase fluctuations three times more rapidly. Example signal interferograms are shown in Supplementary Fig. 4. In one channel interferograms are measured with and in the other one without the pulse stacking.
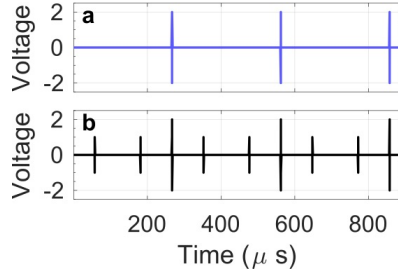
Supplementary Fig. 4 Example signal interferograms. **(a)** DCS interferogram used for spectroscopy analysis. **(b)** Reference signal containing three interferograms per Δf_{rep} period, used to effectively triple the phase sampling rate.

5 Relative intensity noise measurements

The RIN measurement scheme, which is adapted from the one we described in [3], uses two measurements (one for low noise frequencies and one for high noise frequencies) and stitches them together to get high sensitivity across the whole frequency range. The baseband noise on the photocurrent generated by an InGaAs photodiode is measured on a signal source analyzer (SSA) (Keysight Technologies E5052B). To illustrate the relation of the pump and OPO RIN, the measurements of both the pump beams and the signal beams are given. For the RIN measurements, the following average powers were sent to the photodiode: 6.9 mW (pump 1), 5.4 mW (pump 2), 4.6 mW (signal 1), and 3.0 mW (signal 2). The RIN power spectral density (PSD) for both the SSL and the OPO spanning from 10 Hz to 10 MHz is displayed in Supplementary Fig. 5a, and the corresponding integrated RIN spectrum is shown in Supplementary Fig. 5b. We see that the RIN reaches the measurement noise floor at about 1 MHz. For both the pump laser and the OPO, the RIN is lower than –160 dBc/Hz beyond 1 MHz offset frequencies. For the OPO, the integrated RIN is 0.031% (signal 1) and 0.030% (signal 2) when integrated from 10 Hz to 10 MHz. Due to the absence of available data in literature, a comparison of the RIN performance to other dual-comb OPO approaches is not possible.
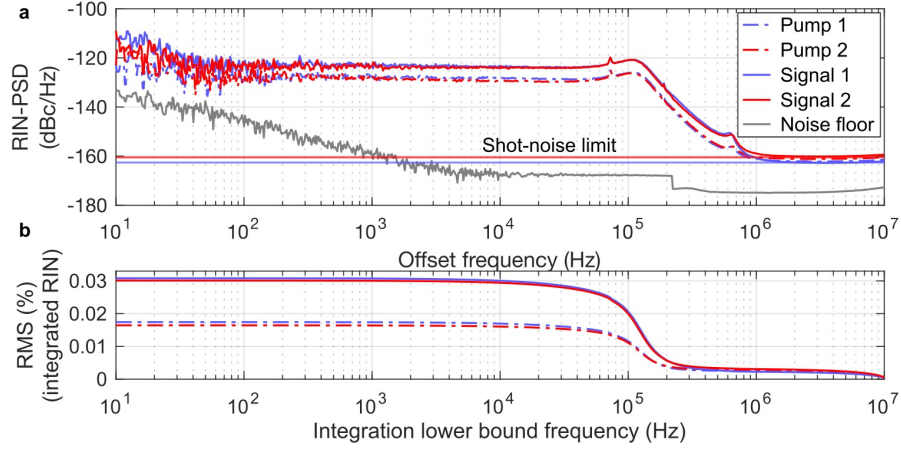
Supplementary Fig. 5 Intensity noise characterization of the single-cavity dual-comb system based on baseband measurements for the Yb:YAG laser (dash-dotted: pump 1 in blue, pump 2 in red) and for the signal beams (solid: signal 1 in blue, signal 2 in red). To determine the measurement noise floor, the optical input to the photodiode was blocked and the resulting power spectral density was scaled according to the typical incident power in the unblocked case (4.5 mW). The resulting effective RIN noise floor is at around -175 dBc/Hz (grey); it is well below the measured RIN values. **(a)** RIN-PSD. The straight solid lines indicate the shot noise limit for the signal measurements: -163 dBc/Hz (signal 1, blue), -160.5 dBc/Hz (signal 2, red). **(b)** Integrated RIN-PSD with the integration interval from 10 Hz to 10 MHz. Stitching frequency: 220 kHz.

6 Comparison of the measured figure of merit with the literature

In Supplementary Fig. 6, we compare the figure of merit (FOM) calculated according to Eq. (5) in [4] for the CCS measurement shown in Supplementary Fig. 10 (indicated by the blue star) with results obtained in the literature (denoted by the last name of the first author and the year of publication). We limit our comparison to dual-comb results obtained in a travelling wave configuration and only list milestone results aiming for a high FOM.
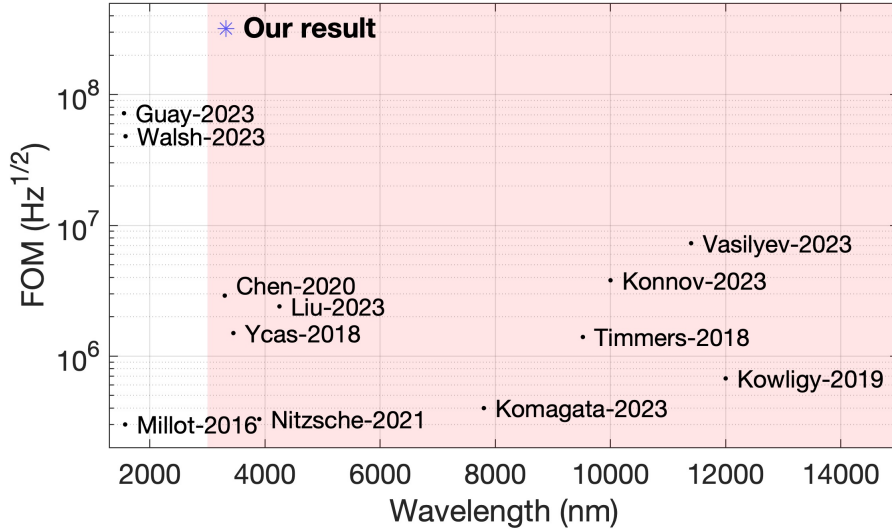
Supplementary Fig. 6 Figure of merit for DCS measurements in a traveling wave configuration. Our result obtained in the CCS measurement shown in Supplementary Fig. 10 is indicated by a blue star. We calculate the FOM according to Eq. (5) in [4]. The results from the literature are denoted by the last name of the first author and the year of publication. The area shaded in red marks the mid-IR wavelength band.

Our figure of merit is a factor of five higher than the highest so far demonstrated FOM [4]. A FOM of 7.2×10^7 Hz$^{1/2}$ was obtained at a center wavelength of 1550 nm by sending 47 mW total power to a balanced pair of detectors that were fast enough to allow for correction of the introduced non-linearity. The measurement in [4] was limited by the RIN of the laser source used, so there is room for further improvement by combining high-power detectors with bulk solid-state laser-based light sources that are not limited by RIN. Note that the Optica review paper [5] referred to a FOM of 2×10^8 Hz$^{1/2}$ for a measurement reported in [6], but as discussed more recently by authors from the same group in [4] this value was an overestimate due to not accounting for the spectral shape.

In comparison to measurements in the mid-IR (center wavelength > 3000 nm), we achieve an improvement of the FOM by a factor of 50 compared to the highest so far demonstrated FOM [7]. The authors demonstrate DCS measurements with ultra-broadband instantaneous bandwidth in the difficult longwave infrared wavelength band > 6000 nm employing a high power and low-noise solid state laser source emitting at 2.4 µm for intra-pulse difference frequency generation.

In comparison to the highest so far demonstrated FOM using a detection scheme based on up-conversion [8], we achieve an improvement by a factor of 150. The remaining references shown in Supplementary Fig. 6 are listed in the order of their publication [9–17].

References

[1] Gayer, O., Sacks, Z., Galun, E., Arie, A.: Temperature and wavelength dependent refractive index equations for MgO-doped congruent and stoichiometric LiNbO3. Appl. Phys. B **91**(2), 343–348 (2008) https://doi.org/10.1007/s00340-008-2998-2

[2] Newbury, N.R., Coddington, I., Swann, W.: Sensitivity of coherent dual-comb spectroscopy. Optics Express **18**(8), 7929–7945 (2010) https://doi.org/10.1364/OE.18.007929

[3] Pupeikis, J., Willenberg, B., Camenzind, S.L., Benayad, A., Camy, P., Phillips, C.R., Keller, U.: Spatially multiplexed single-cavity dual-comb laser. Optica **9**(7), 713–716 (2022) https://doi.org/10.1364/OPTICA.457787

[4] Guay, P., Walsh, M., Tourigny-Plante, A., Genest, J.: Linear dual-comb interferometry at high power levels. Optics Express **31**(3), 4393–4404 (2023) https://doi.org/10.1364/OE.481671

[5] Coddington, I., Newbury, N., Swann, W.: Dual-comb spectroscopy. Optica **3**(4), 414–426 (2016) https://doi.org/10.1364/OPTICA.3.000414

[6] Roy, J., Deschênes, J.-D., Potvin, S., Genest, J.: Continuous real-time correction and averaging for frequency comb interferometry. Optics Express **20**(20), 21932–21939 (2012) https://doi.org/10.1364/OE.20.021932

[7] Vasilyev, S., Muraviev, A., Konnov, D., Mirov, M., Smolski, V., Moskalev, I., Mirov, S., Vodopyanov, K.: Longwave infrared (6.6-11.4 µm) dual-comb spectroscopy with 240,000 comb-mode-resolved data points at video rate. Optics Letters **48**(9), 2273–2276 (2023) https://doi.org/10.1364/OL.477346

[8] Liu, M., Gray, R.M., Costa, L., Markus, C.R., Roy, A., Marandi, A.: Mid-infrared cross-comb spectroscopy. Nature Communications **14**(1), 1044 (2023) https://doi.org/10.1038/s41467-023-36811-7

[9] Millot, G., Pitois, S., Yan, M., Hovhannisyan, T., Bendahmane, A., Hänsch, T.W., Picqué, N.: Frequency-agile dual-comb spectroscopy. Nature Photonics **10**(1), 27–30 (2016) https://doi.org/10.1038/nphoton.2015.250

[10] Ycas, G., Giorgetta, F.R., Baumann, E., Coddington, I., Herman, D., Diddams, S.A., Newbury, N.R.: High-coherence mid-infrared dual-comb spectroscopy spanning 2.6 to 5.2 µm. Nature Photonics **12**(4), 202–208 (2018) https://doi.org/10.1038/s41566-018-0114-7

[11] Timmers, H., Kowligy, A., Lind, A., Cruz, F.C., Nader, N., Silfies, M., Ycas, G., Allison, T.K., Schunemann, P.G., Papp, S.B., Diddams, S.A.: Molecular fingerprinting with bright, broadband infrared frequency combs. Optica **5**(6), 727–732 (2018) https://doi.org/10.1364/OPTICA.5.000727

[12] Kowligy, A.S., Timmers, H., Lind, A.J., Elu, U., Cruz, F.C., Schunemann, P.G., Biegert, J., Diddams, S.A.: Infrared electric field sampled frequency comb spectroscopy. Sci. Adv. **5**(6), 8794 (2019) https://doi.org/10.1126/sciadv.aaw8794

[13] Nitzsche, L., Goldschmidt, J., Kiessling, J., Wolf, S., Kühnemann, F., Wöllenstein, J.: Tunable dual-comb spectrometer for mid-infrared trace gas analysis from 3 to 4.7 µm. Optics Express **29**(16), 25449–25461 (2021) https://doi.org/10.1364/OE.428709

[14] Chen, Z., Hänsch, T.W., Picqué, N.: Upconversion mid-infrared dual-comb spectroscopy. arXiv **2003.06930** (2020)

[15] Komagata, K.N., Wittwer, V.J., Südmeyer, T., Emmenegger, L., Gianella, M.: Absolute frequency referencing for swept dual-comb spectroscopy with midinfrared quantum cascade lasers. Physical Review Research **5**(1), 013047 (2023) https://doi.org/10.1103/PhysRevResearch.5.013047

[16] Walsh, M., Guay, P., Genest, J.: Unlocking a lower shot noise limit in dual-comb interferometry. APL Photonics **8**(7), 071302 (2023) https://doi.org/10.1063/5.0153724

[17] Konnov, D., Muraviev, A., Vasilyev, S., Vodopyanov, K.: High-resolution frequency-comb spectroscopy with electro-optic sampling and instantaneous octave-wide coverage across mid-ir to thz at a video rate. APL Photonics **8**(11) (2023) https://doi.org/10.1063/5.0165879